The Roles of γ1 Heavy Chain Membrane Expression and Cytoplasmic Tail in IgG1 Responses

Tsuneyasu Kaisho,*† Frieder Schwenk, Klaus Rajewsky

In antibody responses, B cells switch from the expression of immunoglobulin (Ig) μ and δ heavy (H) chains to that of other Ig classes (α, γ, or ε), each with a distinct effector function. Membrane-bound forms of α, γ, and ε, but not μ and δ, have highly conserved cytoplasmic tails. Mutant mice unable to express membrane γ1 H chains or producing tailless γ1 H chains failed to generate efficient IgG1 responses and IgG1 memory. H chain membrane expression after class switching is thus required for these functions, and class switching equips the B cell antigen receptor with a regulatory cytoplasmic tail that naïve B cells lack.

The B cell antigen receptor (BCR) initially expressed on B lymphocytes consists of membrane Ig (mIg) made up of μ heavy (H) chains plus light chains, associated with the Ig-α–Ig-β heterodimer (*1*). Because μ H chains have a cytoplasmic tail of only three residues, signaling through the BCR depends on the cytoplasmic tails of Ig-α and Ig-β. On stimulation with antigen, B cells often undergo isotype switching (*2*) leading to the expression of H chains of other classes. These other H chains are not only present in secreted antibodies but can also be expressed as a component of the BCR on the cell surface. Indeed, memory B cells, produced in T cell–dependent antibody responses, classically express BCRs that contain H chains of classes other than μ or δ. The membrane forms of γ, ε, and α H chains differ conspicuously from those of μ and δ in that they possess cytoplasmic tails of 28 (γ, ε) and 14 (α) amino acids, which are highly conserved in evolution (*1*). This raises the possibility that the BCRs expressed on naïve and memory B cells exhibit distinct signaling properties.

Memory B cells generated in response to protein antigens typically express γ1 chains on the cell surface. We generated two types of mouse mutants: one unable to express γ1 chains on the membrane ($IgG1^{\Delta m}$) and the other able to express mIgG1 but lacking the γ1 cytoplasmic tail ($IgG1^{\Delta tail}$). The generation of the $IgG1^{\Delta m}$ and $IgG1^{\Delta tail}$ mutations by gene targeting is depicted in Fig. 1. A single vector was used to target the γ1 locus of embryonic stem (ES) cells bearing the IgH^a allele (*3*). The $IgG1^{\Delta tail}$ mutation was generated by Cre recombinase–mediated deletion of the neomycin resistance (*neo*^{r}) gene from the targeted locus (*4*). The $IgG1^{\Delta tail}$ mutation leads to the production of γ1 chains with a truncated cytoplasmic tail of three amino acids, identical to that of μ chains. The $IgG1^{\Delta tail}$ mutation was transmitted into the mouse germ line, and the $IgG1^{\Delta m}$ mutation was derived from it by a second step of Cre-mediated deletion in vivo, using the *deleter* strain (*5*).

The effects of the two mutations on B cell development and function were assessed in mice heterozygous or homozygous for either mutation. Heterozygous animals carried a wild-type allele of *b* allotype, the products of which can be distinguished from those of the mutant *a* alleles by anti-allotypic antibodies. All animals generated IgM- and IgD-bearing B cells in normal numbers. When B cells from homozygous mutants of either type were activated in vitro by bacterial lipopolysaccharide (LPS) in the presence of interleukin 4 (IL-4) (*6*), they switched to IgG1 expression with equal efficiency as the wild type. This was determined by intracellular staining of the activated cells after fixation and incubation with antibodies to IgG1 (Fig. 2A). Cells from the same cultures were also stained for IgG1 surface expression (Fig. 2B). No staining was observed in the case of the $IgG1^{\Delta m}$ mutant, as expected. In the case of $IgG1^{\Delta tail}$, surface IgG1-positive cells were seen at the expected frequency. However, the average staining intensity was roughly threefold less than that of wild-type cells, for reasons that remain to be explored.

Marked differences were seen between mutants and the wild type at the level of IgG1 responses. When heterozygous mutants were immunized with a T cell–dependent antigen, chicken γ-globulin (CG) coupled to 4-hydroxy-3-nitro-phenylacetyl (NP), they produced far less NP-specific IgG1 from the mutant than from the wild-type alleles. The differences were more pronounced for the $IgG1^{\Delta m}$ than for the $IgG1^{\Delta tail}$ mutant and most severe in the secondary response, where in both cases, IgG1 from the mutant alleles was hardly detectable (*7*). In homozygous mutants (Fig. 3), the serum IgG1 concentrations were reduced by factors of 24 for $IgG1^{\Delta tail}$ and 71 for $IgG1^{\Delta m}$, compared with control mice of strain 129 (Fig. 3A). Other IgG classes were unaffected. Upon immunization with NP-CG, both mutant strains produced strongly impaired primary and secondary IgG1 responses, which were about two orders of magnitude below the control in the case of the $IgG1^{\Delta m}$ and about one order of magnitude in that of the $IgG1^{\Delta tail}$

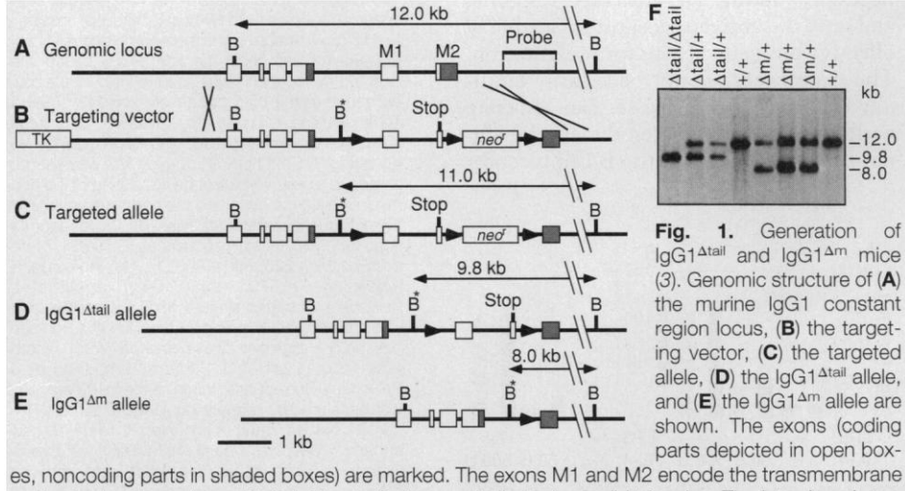

Fig. 1. Generation of $IgG1^{\Delta tail}$ and $IgG1^{\Delta m}$ mice (*3*). Genomic structure of (**A**) the murine IgG1 constant region locus, (**B**) the targeting vector, (**C**) the targeted allele, (**D**) the $IgG1^{\Delta tail}$ allele, and (**E**) the $IgG1^{\Delta m}$ allele are shown. The exons (coding parts depicted in open boxes, noncoding parts in shaded boxes) are marked. The exons M1 and M2 encode the transmembrane and cytoplasmic regions of IgG1. The *loxP* sites are indicated as solid triangles. The introduced stop codon (stop), the lengths of diagnostic restriction fragments (arrows), and the probe used for Southern (DNA) blot analysis (black bar) are shown. B, Bam HI. (**F**) Southern blot analysis. Bam HI digestion of genomic DNA yields fragments of 12.0, 9.8, and 8.0 kb corresponding to the wild-type (+), $IgG1^{\Delta tail}$ (Δtail), and $IgG1^{\Delta m}$ (Δm) allele, respectively.

Institute for Genetics, University of Cologne, Weyertal 121, D-50931 Cologne, Germany.

*To whom correspondence should be addressed.
†Present address: Department of Biochemistry, Hyogo College of Medicine, Hyogo 663, Japan. E-mail: tkaisho@home.hyo-med.ac.jp

mutant (Fig. 3, C and D). Again, other Ig classes were unaffected (Fig. 3, E and F). Affinity maturation of IgG1 antibodies in the course of the response was less efficient in the IgG1$^{\Delta tail}$ mutant than in the controls (Fig. 3B). For the IgG1$^{\Delta m}$ mutant, the low antibody titers did not allow us such an analysis.

Our results demonstrate that B cells expressing either the IgG1$^{\Delta m}$ or the IgG1$^{\Delta tail}$ mutation are unable to mount efficient primary and secondary IgG1 responses in vivo, either in competition with B cells expressing wild-type IgG1 (the heterozygous mutant animals) or in the absence of such cells (Fig. 3). Assuming that these responses depend on the expansion of cells expressing IgG1 in their BCR as earlier work suggests (8), this result is expected for the IgG1$^{\Delta m}$ mutant, which is unable to express IgG1 at the surface. In the case of the IgG1$^{\Delta tail}$ mutant, the impaired response could be because of inefficient expansion or persistence of surface IgG1-bearing cells, impaired terminal differentiation into antibody secreting cells, or both. We have approached this matter by determining the numbers of surface IgG1-positive splenic B cells in homozygous mutant mice, either disregarding their antigen-binding specificity or as IgG1^{+}NP^{+}B cells during the anti-NP response. A well-defined subset of IgG1-positive cells was identified 4 weeks after immunization with NP-CG in both mutant and wild-type mice (Fig. 4) (9). In contrast to what was seen in the case of LPS-activated blasts (Fig. 2), the intensity of staining for mIgG1 did not apparently differ between the wild type and the mutant for most of the cells of this subset, although there may be a small fraction of bright cells in the wild type that are missing in the mutant (Fig. 4, A and B). A minority of the IgG1-positive cells specifically bind NP-carrier conjugates (Fig. 4, C and D), in agreement with earlier studies (*10*). These cells represent typical memory B cells selected in the germinal center reaction upon primary immunization with T cell–dependent antigens (*11*). The mutant animal analyzed in Fig. 4 harbored significantly (approximately 25 times) less IgG1-positive cells than did its wild-type counterpart. As a rule and irrespective of intentional immunization, the mutants displayed roughly ten times fewer IgG1-positive cells in their spleens than did the wild type (Table 1).

We conclude that surface IgG1 expression is essential for the generation of efficient primary and secondary IgG1 responses and that both the primary IgG1 response as well as the expansion or maintenance, or both, of IgG1-bearing memory B cells depend strongly on the cytoplasmic tail of the

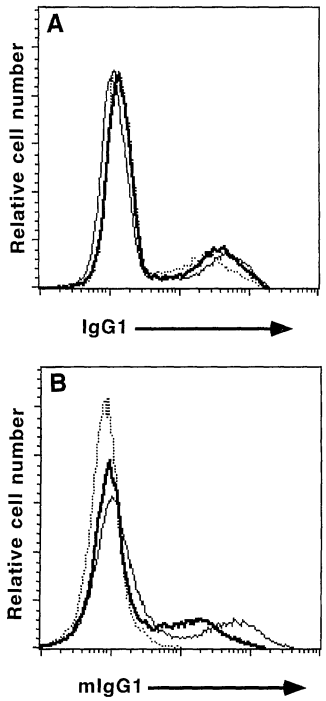

Fig. 2. Flow cytometric analysis of spleen cells derived from wild-type (thin lines), IgG1$^{\Delta tail/\Delta tail}$ (bold lines), and IgG1$^{\Delta m/\Delta m}$ mice (dotted lines) after in vitro stimulation with LPS and IL-4 (*17*). Shown are (**A**) staining of intracellular IgG1 and (**B**) IgG1 surface expression.

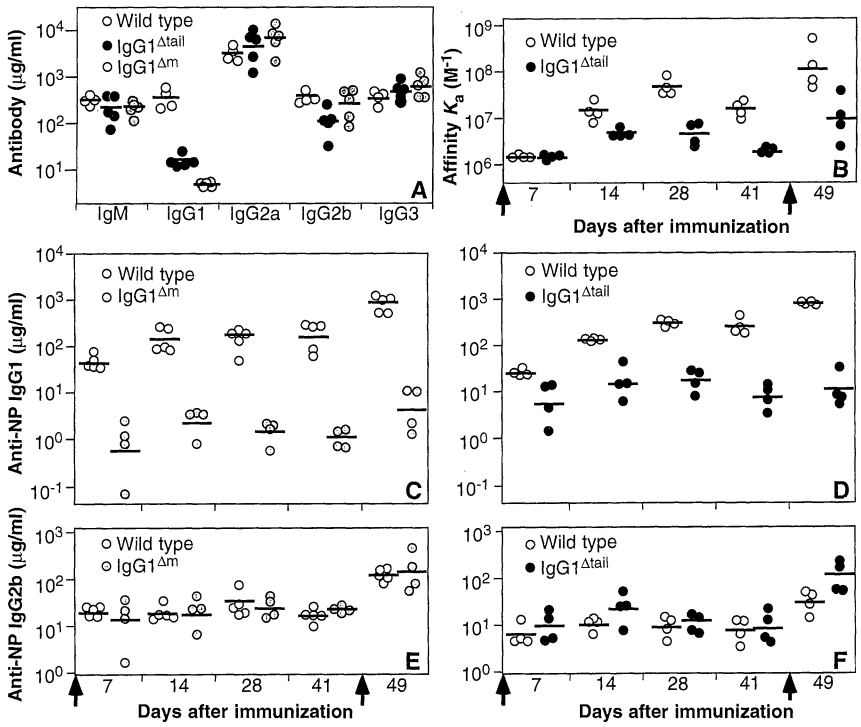

Fig. 3. Immune response in wild-type (open dots), IgG1$^{\Delta tail/\Delta tail}$ (black dots), and IgG1$^{\Delta m/\Delta m}$ (gray dots) mice (*18*). (**A**) Serum levels of Ig isotypes are shown for unimmunized wild-type, IgG1$^{\Delta tail/\Delta tail}$, and IgG1$^{\Delta m/\Delta m}$ mice. (**B**) Affinity maturation of NP-specific IgG1 serum antibody in wild-type and IgG1 mice is shown at various days after the first immunization. (C to F) NP-specific IgG1 (**C** and **D**) and IgG2b (**E** and **F**) serum levels in wild-type, IgG1$^{\Delta tail/\Delta tail}$, and IgG1$^{\Delta m/\Delta m}$ mice. Immunizations at day 0 and day 42 are indicated by arrows. Bars indicate mean values.

Fig. 4. Representative flow cytometric analyses of mIgM^{-}/mIgD^{-} spleen cells from wild-type (A and C) and IgG1$^{\Delta tail/\Delta tail}$ (B and D) mice at day 28 after immunization with NP-CG. (**A**) and (**B**) Histograms showing surface IgG1 expression. Bars indicate the mIgG1-positive populations. (**C**) and (**D**) NP-binding versus mIgG1 expression. NP-binding and nonbinding mIgG1 positive cells are framed. In dot plots, 10^5 lymphocytes [as defined by forward and side scatters (*19*)] were collected, and mIgM^{-}/mIgD^{-} cells were analyzed. For the histograms, 2 million lymphocytes were collected, and the bulk of mIgG1-negative cells (as indicated by the leftmost vertical lines of dot plots) were excluded.

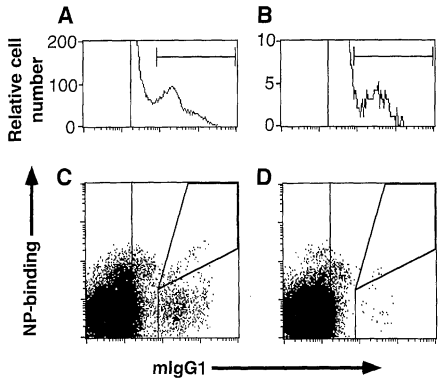

γ1 chain. Achatz *et al.* (*12*) have reached similar conclusions for the IgE response, suggesting that IgG, IgE, and perhaps IgA responses follow similar rules.

How could the cytoplasmic tail of the γ1 chain and perhaps other H chains exert its function? One possibility is that it stabilizes IgG1 surface expression (Fig. 2), allowing more efficient triggering of IgG1-expressing cells by antigen. However, as the level of IgG1 surface expression appeared to be close to normal in memory cells of IgG1$^{\Delta tail}$ mice (Fig. 4), we favor the view that the tail is directly involved in the mechanism by which IgG1-expressing B cells are triggered into the response. Weiser *et al.* (*13*) have shown that transformed B cells expressing an IgG2a BCR require the cytoplasmic tail of γ2a (and specifically a tyrosine-based motif in this structure, which is also present in γ1) for efficient presentation of antigen to T cells, following sIg-mediated internalization. As IgG1 responses are usually T cell–driven, inefficient presentation of antigen to T cells by B cells expressing tail-less γ1 chains could explain the observed phenotype of the IgG1$^{\Delta tail}$ mutant. Thus, upon switching to IgG1 expression in the T cell–driven germinal center reaction, further expansion and mutation of the antigen-activated cells would become dependent on IgG1-BCR–mediated antigen presentation and, therefore, the cytoplasmic tail of the γ1 chain. This would explain the inefficiency of affinity maturation and memory cell generation in the mutant.

The cytoplasmic tails of γ chains may by themselves be unable to transduce a signal into the cell (*14*). However, if the triggering of IgG-expressing germinal center and memory B cells [which are known to be potent antigen-presenting cells (*15*)] depends exclusively on their interaction with activated T helper cells, then the activation of these B cells would be mediated by the cytoplasmic tails of the γ chains instead of the Ig-α–Ig-β heterodimer involved in the activation of IgM-expressing naïve B cells. Consistent with this possibility is the finding that in cultured cells, IgG can be expressed at the cell surface in the absence of Ig-α and Ig-β (*16*). Whether this is the case in murine IgG1-positive memory B cells is presently unknown.

On the basis of our results and those of Achatz *et al.* (*12*) and of Weiser *et al.* (*13*), and given the structural differences between the cytoplasmic tails of antibody H chains of different classes (associated with different effector functions), these structures whose significance was previously elusive, emerge as important regulators of the class distribution of antibody responses and of immunological memory, and thus as potential targets for therapeutic intervention.

Table 1. NP-binding and mIgG1-expressing cell populations in the spleen of wild-type and IgG1$^{\Delta tail/\Delta tail}$ mice before and after immunization with NP-CG. We analyzed 10^5 cells as described in Fig. 4. Results are expressed as percentages of total spleen cells. Mean values and standard deviations are shown, except for the results obtained at day 49.

Day (number of animals)	NP$^+$mIgG1$^+$	All mIgG1$^+$
	Wild-type mice	
0* (4)	<0.01	0.15 ± 0.05
14 (6)	0.18 ± 0.08	0.90 ± 0.18
28 (5)	0.08 ± 0.03	0.72 ± 0.21
49 (2)	0.05, 0.05	0.53, 0.58
	IgG1$^{\Delta tail/\Delta tail}$ mice	
0 (4)	<0.01	0.01 ± 0.01
14 (6)	0.02 ± 0.01	0.08 ± 0.07
28 (5)	0.01 ± 0.01	0.06 ± 0.03
49 (2)	0.01, <0.01	0.02, 0.02

*Results from unimmunized mice.

REFERENCES AND NOTES

1. M. Reth, *Annu. Rev. Immunol.* **10**, 97 (1992).
2. C. Esser and A. Radbruch, *Ibid.* **8**, 717 (1990).
3. To generate the gene-targeting vector, the codon encoding the fourth amino acid (TGG, tryptophan) of the IgG1 cytoplasmic tail was converted into a stop codon (TGA) by polymerase chain reaction–mediated mutagenesis. A *neo*^{r} gene flanked by two *loxP* sites [L. Ferradini *et al.*, *Science* **271**, 1416 (1996)] was placed downstream of the stop codon. The third *loxP* site was inserted 5′ of the two transmembrane exons. A 7.3-kb DNA segment including the exons encoding the extracellular and transmembrane part of the mIgG1 constant region [T. Honjo *et al.*, *Cell* **18**, 559 (1979)] and a 1-kb fragment containing the polyadenylation signal were used as the long arm and the short arm of homology, respectively. To confirm that the targeting vector encoded a functional Cγ1 region, a fragment including all exons that encode the extracellular and transmembrane part of Cγ1 was inserted into an expression vector containing the IgH promoter and a rearranged V_H gene [U. Weiss and K. Rajewsky, *J. Exp. Med.* **172**, 1681 (1990)]. The resulting construct was transfected into the IgG1-negative, κ-positive B cell line K46 [K. J. Kim, C. Kanellopoulos-Langevin, R. M. Merwwin, D. H. Sachs, R. Asofsky, *J. Immunol.* **122**, 549 (1979)]. All transfectants tested showed surface expression of IgG1, indicating that the targeting vector allows expression of truncated mIgG1 on the cell surface. E14-1 ES cells [R. Kühn, K. Rajewsky, W. Müller, *Science* **254**, 707 (1991)] were transfected with the Sal I–linearized targeting vector by electroporation. Double selection with G418 and gancyclovir resulted in seven homologous recombinants out of 148 double-resistant clones. Three out of seven homologous recombinants contained the upstream *lox P* site (Fig. 1C). The *lox P*–flanked *neo*^{r} gene was removed from the targeted allele by Cre-mediated recombination in ES cells to generate the IgG1$^{\Delta tail}$ mutation. ES cell clones heterozygous for the IgG1$^{\Delta tail}$ mutation were injected into C57BL/6 blastocysts. The IgG1$^{\Delta m}$ strain harboring the deletion of the IgG1 transmembrane exon was generated by crossing IgG1$^{\Delta tail}$ mice to the *deleter* strain (*5*). Sequence analysis of tail DNA from IgG1$^{\Delta tail/\Delta tail}$ mice confirmed that the stop codon had been introduced and revealed no unexpected mutations in any of the exons encoding the IgG1 constant region.
4. H. Gu, Y. Zou, K. Rajewsky, *Cell* **73**, 1155 (1993).
5. F. Schwenk, U. Baron, K. Rajewsky, *Nucleic Acids Res.* **23**, 5080 (1995).
6. J. E. Layton, E. S. Vitteta, J. W. Uhr, P. H. Krammer, *J. Exp. Med.* **160**, 1850 (1984).
7. T. Kaisho, F. Schwenk, K. Rajewsky, data not shown.
8. K. Okumura, M. H. Julius, T. Tsu, L. A. Herzenberg, L. A. Herzenberg, *Eur. J. Immunol.* **6**, 467 (1976); H. Shan, M. Schlomchik, M. Weigert, *J. Exp. Med.* **172**, 531 (1990).
9. For the analysis of spleen cells, mice were immunized intraperitoneally (i.p.) with 100 μg of alum-precipitated NP_{30}-CG. Single-cell suspensions were stained with a digoxigenin-conjugated rat monoclonal antibody (mAb) to murine IgG1 (Miltenyi Biotec, Bergisch Gladbach, Germany) and NP_{14}–bovine serum albumin (5 μg/ml). Cells were washed and incubated with fluorescein isothiocyanate (FITC)–conjugated sheep anti-digoxigenin Fab fragments (Boehringer, Mannheim), the phycoerythrin-conjugated mAb R33-24-12 to IgM [R. Grützman, thesis, University of Cologne, Germany (1981)], the phycoerythrin-conjugated mAb 1.3-5 to IgD [J. Roes, W. Müller, K. Rajewsky, *J. Immunol. Methods* **183,** 231 (1995)], and the allophycocyanin-conjugated mAb S43 to NP [M. Reth, G. J. Hämmerling, K. Rajewsky, *Eur. J. Immunol.* **8**, 393 (1978)]. Cells were analyzed on a FACStar (Becton Dickinson, San Jose, CA). Dead cells were excluded by propidium iodide staining.
10. B. Pulendran, K. G. C. Smith, G. J. V. Nossal, *J. Immunol.* **155**, 1141 (1995).
11. K. Rajewsky, *Nature* **381**, 751 (1996).
12. G. Achatz, L. Nitschke, M. C. Lamers, *Science* **276**, 409 (1997).
13. P. Weiser, R. Müller, U. Braun, M. Reth, *Ibid.*, p. 407.
14. K. M. Kim, G. Alber, P. Weiser, M. Reth, *Eur. J. Immunol.* **23**, 911 (1993).
15. Y.-J. Liu *et al.*, *Immunity* **2**, 239 (1995).
16. A. R. Venkitaraman *et al.*, *Nature* **352**, 777 (1991); P. Weiser, C. Riesterer, M. Reth, *Eur. J. Immunol.* **24**, 665 (1994).
17. Spleen cells (10^6 cells/ml) were cultured in complete Roswell Park Memorial Institute medium supplemented with LPS (40 μg/ml) and 10% culture supernatant of an IL-4–expressing NIH 3T3 line [S. Jung, K. Rajewsky, A. Radbruch, *Science* **259**, 984 (1993)]. After 3 days of culture, cells were harvested, incubated with the digoxigenin-conjugated rat mAb to murine IgG1 (Miltenyi Biotec, Bergisch Gladbach, Germany), and stained by FITC–conjugated sheep anti-digoxigenin Fab fragments (Boehringer, Mannheim). Intracellular staining was performed as described [M. Assenmacher, J. Schmitz, A. Radbruch, *Eur. J. Immunol.* **24**, 1097 (1994)]. Cells were analyzed on a FACScan (Becton Dickinson, San Jose, CA).
18. Eleven-week-old mice were bled and serum Ig isotype concentrations were analyzed by enzyme-linked immunosorbent assay (ELISA) as described [J. Roes and K. Rajewsky, *J. Exp. Med.* **177**, 45 (1993)]. Note that genetically, homozygous mutants are a mixture of strains 129 and C57BL/6, but that IgG1 levels do not significantly differ between those strains (T. Kaisho, F. Schwenk, K. Rajewsky, unpublished observations). Before immunization, NP-specific IgG1 and IgG2b serum titers were below 0.1 and 0.8 μg/ml, respectively. Mice were immunized with 100 μg of alum-precipitated NP_{30}-CG. A secondary i.p. immunization was performed 6 weeks later, using 5 μg of NP_{30}-CG dissolved in phosphate-buffered saline. Mice were bled and the serum titers of NP-specific IgG1 and IgG2b were determined by ELISA as described by Roes and Rajewsky. Bound Ig was detected by the biotinylated mouse mAb Ig4a(20.9) to mouse IgG1^a [V. T. Oi and L. A. Herzenberg, *Mol. Immunol.* **16**, 1005 (1979)] or a goat anti-mouse IgG2b polyclonal serum (Southern Biotechnology Associates, Birmingham, AL). NP-specific IgG1 of low and high affinity were measured by ELISA with plates coated with, respectively, NP_{14} and NP_4 bovine serum albumin, and the affinity of NP-specific IgG1 was calculated as described by Roes and Rajewsky.
19. I. Förster, P. Vieira, K. Rajewsky, *Int. Immunol.* **1**, 321 (1989).

20. We thank R. Lamers and M. Reth for communicating results before publication. We also thank C. Uthoff-

Hachenberg and C. Göttlinger for competent technical help, W. Müller for the method of detecting NP-specific mIgG1-positive cells, R. C. Rickert and A. Tarakhovsky for critical reading of the manuscript, and U. Ringeisen for graphical work. Supported by fellowships from the Human Frontier Science Programme (HFSP) and the Alexander von Humboldt Foundation to T.K. and by grants from the Deutsche Forschungsgemeinschaft through SFB 243, the HFSP, and the Land Nordrhein-Westfalen. F.S. was supported by a stipend of the Boehringer Ingelheim Fonds.

22 November 1996; accepted 10 February 1997

Solution Structure of 3-Oxo-Δ^5-Steroid Isomerase

Zheng Rong Wu, Soheila Ebrahimian, Michael E. Zawrotny, Lora D. Thornburg, Gabriela C. Perez-Alvarado, Paul Brothers, Ralph M. Pollack,* Michael F. Summers*

The three-dimensional structure of the enzyme 3-oxo-Δ^5-steroid isomerase (E.C. 5.3.3.1), a 28-kilodalton symmetrical dimer, was solved by multidimensional heteronuclear magnetic resonance spectroscopy. The two independently folded monomers pack together by means of extensive hydrophobic and electrostatic interactions. Each monomer comprises three α helices and a six-strand mixed β-pleated sheet arranged to form a deep hydrophobic cavity. Catalytically important residues Tyr^{14} (general acid) and Asp^{38} (general base) are located near the bottom of the cavity and positioned as expected from mechanistic hypotheses. An unexpected acid group (Asp^{99}) is also located in the active site adjacent to Tyr^{14}, and kinetic and binding studies of the Asp^{99} to Ala mutant demonstrate that Asp^{99} contributes to catalysis by stabilizing the intermediate.

Various biological reactions proceed by enzymatic cleavage of a C-H bond adjacent to a carbonyl or carboxyl group, leading to an enol or enolate intermediate that is subsequently reprotonated at the same or an adjacent carbon (*1*). Thermodynamic and kinetic barriers associated with these processes can be very large, requiring the enzymes to provide up to 20 kcal/mol of transition state stabilization (*2*). An important member of this class of enzymes is 3-oxo-Δ^5-steroid isomerase (Δ^5-3-ketosteroid isomerase, KSI, E.C. 5.3.3.1), which is among the most proficient enzymes known (*3*) and has served as a paradigm for enzymatic enolizations since its discovery in 1955 (*4*). This enzyme catalyzes the isomerization of various β,γ-unsaturated 3-oxosteroids to their conjugated isomers at nearly a diffusion-controlled rate (*5*).

Extensive kinetic and mutagenesis studies indicate that catalysis proceeds by predominant abstraction of the steroid C4-β proton by Asp^{38}, with stabilization of the resulting dienolate intermediate by a hydrogen bond from Tyr^{14}-OH (*6–10*). Nuclear magnetic resonance (NMR) studies have led to the conclusion that the intermediate is stabilized by a single low barrier hydrogen bond (LBHB) (*11*), and it has been further proposed that the entire rate enhancement by KSI can be quantitatively attributed to residues Asp^{38} and Tyr^{14} (*11*). Nevertheless, fluorescence titration of the Tyr^{14}-OH suggests the presence of an active site residue with pK_a of 9.5 (*12*), and there is evidence that this unknown group is catalytically important (*13, 14*). There is also a substantial contribution to the rate of enzymatic proton transfer by Phe^{101} that has yet to be satisfactorily explained (*15*).

Despite more than 20 years of effort, high-resolution structural information that would identify all of the active site residues and facilitate a complete mechanistic analysis has been lacking. Crystals of KSI that diffract to 2.7 Å have been reported (*16, 17*), and a three-dimensional (3D) model refined to 6 Å resolution suggested that the substrate binding site is located within a cavity near the dimer interface (*18*). In order to provide a more detailed and independent assessment of the solution structure of KSI, we have determined its complete 3D structure using heteronuclear multidimensional and triple resonance NMR methods.

^{15}N- and $^{15}N,^{13}C$-labeled KSI samples for NMR studies were expressed in *Escherichia coli* and purified under nondenaturing conditions (*19*). Protein aggregation is significant at dimer concentrations greater than 80 μM (*20*), and was inhibited when 90% water and 10% dioxane-d_8 were used as solvent. The introduction of dioxane led to small chemical shift changes (<0.1 ppm) for only a few NMR signals, and to a minor reduction in enzyme activity (*21*), indicating that the protein structure was not significantly altered under these conditions. Gradient-enhanced triple-resonance NMR methods, including four-dimensional $^{15}N,^{13}C$- and $^{13}C,^{13}C$-edited nuclear Overhauser effect (NOE) experiments, were used to assign the backbone and side chain signals (*22*). The observation of 117 of the 119 expected backbone NH correlation signals per polypeptide in the NMR spectra revealed that the protein dimer is structurally symmetric. Intermolecular NOEs were identified by comparing the four-dimensional (4D) NOE NMR data obtained for the uniformly labeled dimer with 3D pulsed-field gradient-edited ^{13}C-filtered–^{12}C-detected NOE data obtained for a heterodimer comprising nonlabeled and $^{15}N,^{13}C$-labeled subunits. For example, the Val^{74}-γ^2CH_3 exhibits intramolecular NOE cross peaks with Val^{74}-γ^1CH_3, -Hβ, -Hα (Fig. 1A), as well as intermolecular cross peaks with Leu^{115}-Hα, -Hγ, -δ^2CH_3 and with Val^{40}-Hβ and -CH_3 protons (Fig. 1B). With this approach, we were able to unambiguously assign 30 intermolecular NOE cross peaks.

A total of 1865 experimental distance restraints identified from the NOE data were used to generate an ensemble of 20 distance geometry structures with the program DIANA (*23*). Statistical information

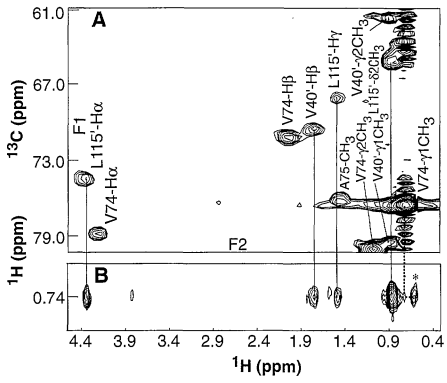

Fig. 1. Nuclear Overhauser effect (NOE) data associated with the Val_{74}-γ^2CH_3 methyl group. (**A**) Selected plane [F4 (^1H) = 0.74 ppm; F3 (13C) = 16.48 ppm] from the 4D $^{13}C,^{13}C$-edited NOE spectrum showing both intermolecular (denoted with primes) and intramolecular dipolar interactions. (**B**) Corresponding plane from the 3D gradient-purged ^{13}C-filtered–^{12}C-detected half-filtered NOE spectrum [F1 (^{13}C) = 16.48 ppm] showing intermolecular NOE correlation signals (* denotes the incompletely suppressed Val^{74}-γ^2CH_3 autopeak doublet).

Z. R. Wu, M. E. Zawrotny, G. C. Perez-Alvarado, M. F. Summers, Howard Hughes Medical Institute and Department of Chemistry and Biochemistry, University of Maryland Baltimore County, 1000 Hilltop Circle, Baltimore, MD 21250.
S. Ebrahimian, L. D. Thornburg, P. Brothers, R. M. Pollack, Department of Chemistry and Biochemistry, University of Maryland Baltimore County, 1000 Hilltop Circle, Baltimore, MD 21250, and Center for Advanced Research in Biotechnology (R. M. Pollack), 9600 Gudelsky Drive, Rockville, MD 20850.
*To whom correspondence should be addressed.